1 Introduction

The science of physics is the study of matter in the universe. Broadly speaking, this study is divided into two tasks: identifying what kinds of matter exist, and understanding the properties of the different types of matter. This thesis presents a study of one of the most common particles of matter in the visible universe: the proton. Specifically, it addresses an important relationship between the components of matter that make up the proton: the quarks and the gluons.

The physical process on which this analysis is based is called “neutrino-nucleon deep-inelastic scattering.” In a scattering experiment, a target composed of one type of particle is exposed to a beam. The particles in the beam are said to “scatter” off of the particles that make up the target. The formula that describes this interaction is

$$\nu_\mu + N \to \mu + X \tag{1.1}$$

The symbol ν refers to the neutrino, which is a light, neutral, weakly-interacting particle; the subscript μ implies that the neutrino is of a particular type: the muon neutrino. The symbol N represents a nucleon, either a proton or a neutron, in the nucleus of an atom. One product of this interaction is a muon, designated by the symbol μ. It is the transformation of the neutral neutrino to a charged muon that labels the event as a “charged-current” event; if the charge of the neutrino remained unchanged as a result of the interaction, it would be a “neutral-current” event. The other result of the interaction is a shower of particles known as hadrons, which result from the break-up of the proton due to the energy transferred to the proton by the incoming neutrino. It is the “hadron shower” that labels the event as “deep-inelastic scattering,” since in elastic scattering the proton remains intact.

This introductory chapter provides the context for the rest of the thesis. The Standard Model of particle physics is described, introducing the quarks and leptons—the constituents of all matter—and the forces by which they interact. The kinematic variables that define the interaction of Equation 1.1 are described. Next, the formalism of deep-inelastic scattering is discussed, starting with the definition of the structure functions in terms of the Standard Model of electroweak interactions, and then connecting the measured structure functions with the theory of Quantum Chromodynamics. The chapter concludes with an overview of the structure-function analysis and this thesis.

1.1 The Standard Model

Over the last three decades, experimental and theoretical efforts in the field of particle physics developed a paradigm known as the Standard Model, which includes the unified theory of electroweak interactions [Wei67, Sal68] along with Quantum Chromodynamics (QCD) [Ynd93], the theory of strong interactions. The sample of charged-current events presented in this thesis are analyzed using the Standard Model, and the theory is shown to be consistent with the data. A fundamental parameter of the Standard Model, the strong coupling constant α_S, is measured in this analysis.

In the Standard Model, all fundamental interactions occur between quarks and leptons, which are fermions, through the exchange of gauge particles, which are bosons. This theoretical edifice has been successful in explaining the ever-growing number of experiments that have been performed to study it. A complete introduction to the Standard Model may be found in textbooks [Per82, Hal84] and only a brief description of the Standard Model follows.

Table 1.1: The quarks and leptons, constituents of matter.

	Charge (units of electron charge)	First Generation	Second Generation	Third Generation
Quarks	+2/3	up (u)	charm (c)	top (t)
	–1/3	down (d)	strange (s)	bottom (b)
Leptons	–1	electron (e)	muon (μ)	tau (τ)
	0	e-neutrino (ν_e)	μ-neutrino (ν_μ)	τ-neutrino (ν_τ)

The fermions of the Standard Model are listed in Table 1.1, where they are grouped into three generations. Each entry in Table 1.1 represents a different "flavor" of particle. Ordinary terrestrial matter is made of particles from the first generation: protons and neutrons carry net up and down quantum numbers, electrons orbit the nuclei of atoms, and electron-(anti)-neutrinos are emitted in nuclear beta decay. The higher-mass fermions of the second and third generations are present in the high-energy environments produced by cosmic rays and particle accelerators. All of the fermions have antimatter partners, which have the same mass but opposite quantum numbers. Of the particles listed, only the ν_τ has not yet been directly observed through their interaction with other matter.

The fermions interact through the exchange of gauge bosons. The mediators of each of the four forces are listed in Table 1.2. All the fermions interact weakly, through the exchange of the Z^0 and $W^\pm$ bosons, known as the intermediate gauge bosons. Electrically-charged particles—that is, all fermions other than the neutrinos—interact electromagnetically, through the exchange of photons. Finally, quarks alone interact strongly and therefore they alone are the fermions that carry strong (or color) charge. Quarks interact strongly by exchanging gluons. Gravity affects all particles, and its carrier is assumed to be the graviton. However, when considering interactions of elementary particles, the effects of gravity are negligible, and gravity is not discussed further.

Table 1.2: Interactions in the Standard Model. The relative strengths of the forces are roughly indicated, for short distance scales of a few *GeV*.

Interaction	Relative strength	Mediator	Participating fermions
strong	1	gluon (g)	quarks
electromagnetic	10^{-2}	photon (γ)	quarks and charged leptons
weak	10^{-5}	Z^0 and $W^{\pm}$	all
gravitational	10^{-42}	graviton (G)	all

The ultimate validity of the Standard Model rests in its ongoing confirmation by experimental data. Up to now, the confirmation has been excellent, and there is no compelling evidence for physics beyond the Standard Model. However, the Standard Model leaves some questions unanswered. For example, the Standard Model has 19 input parameters, which are listed in Table 1.3. Precise measurements of these parameters check the self-consistency of the theory, but offer no insight into the parameters themselves. Physicists expect that an elegant theory beyond the Standard Model would not require such a large number of parameters. Furthermore, the Standard Model does not explain the number of fermions or the generational hierarchy of the quarks and leptons, nor offers any reason for the symmetry that seems to exist between the quark and lepton sectors. And although the Standard Model accommodates CP (charge-conjugation and parity) violating interactions, it offers no explanation of them.

A few mandatory empirical tests of the Standard Model are yet to be completed, most notably the detection of the Higgs particle. Precise measurements of Standard Model parameters may uncover the first discrepancy between the model and observation. However well-established our current Standard Model, there is a need to go beyond it, to explain the questions it cannot answer. New physics may emerge as new generations of

Table 1.3: The number of parameters in the minimal Standard Model. The neutrinos, photons, and gluons are massless.

Type of parameter	Number of parameters
quark masses	6
charged lepton masses	3
CKM mixings	4
Z^0 and $W^{\pm}$ masses	2
Higgs particle mass	1
α_{em} electromagnetic coupling	1
G_F weak coupling	1
α_S strong coupling	1
TOTAL	19

accelerators probe shorter distances and higher energies, or as experiments push existing limits with more precise measurements.

1.2 Neutrino-Nucleon Scattering

Neutrinos make excellent probes for studying the structure of hadrons. They are structureless particles and their electroweak interactions are well understood. Neutrinos are always polarized, and are therefore uniquely suited for studies of the helicity-dependent dynamics of the nucleon constituents.

The Standard Model describes the phenomenology of deep-inelastic scattering well. At high energy, deep-inelastic neutrino-nucleon scattering is interpreted as elastic neutrino-parton scattering. Nucleon structure at high momentum transfers is characterized by parton distribution functions, which describe the nucleon in terms of quarks and gluons using the factorization theorems of Quantum Chromodynamics (QCD) [Sop89]. This

Section introduces the formalism used to describe nucleon structure in terms of parton distributions.

The process of probing the nucleon with neutrinos begins by using the inclusive charged-current data sample to measure the nucleon's structure functions. The structure functions are a complete set of Lorentz scalars that parameterize the unknown structure of the proton. The properties of the structure functions lead to the parton model, which proposes that the nucleon is composed of point-like constituents, partons, that scatter elastically with the neutrino. Finally, the partons are identified with the quarks and gluons of QCD, and QCD describes the parton dynamics. A QCD analysis of the structure function measurements provides a determination of the nucleon's valence and sea quark distributions and gluon distribution, along with a determination of α_S.

1.2.1 The Kinematics of a Charged-Current Neutrino Event

Three kinematic parameters provide a full description of a deep-inelastic scattering event. In this experiment, the three measured parameters of a charged-current event are the muon momentum, p_μ, the angle of the outgoing muon, θ_μ, and the observed energy of the outgoing hadrons, E_{HAD}. From these measured parameters it follows that the neutrino energy is $E = E_\nu = E_{HAD} + E_\mu. + M$.

The kinematic variables of deep-inelastic scattering are shown in Figure 1.1. The lepton is designated by four-momentum k, the hadron system by momentum p, and after scattering their four-momenta are designated by k' and p', respectively. In terms of the experimental quantities each of these four-momenta in the lab system are (M is the mass of the nucleon):

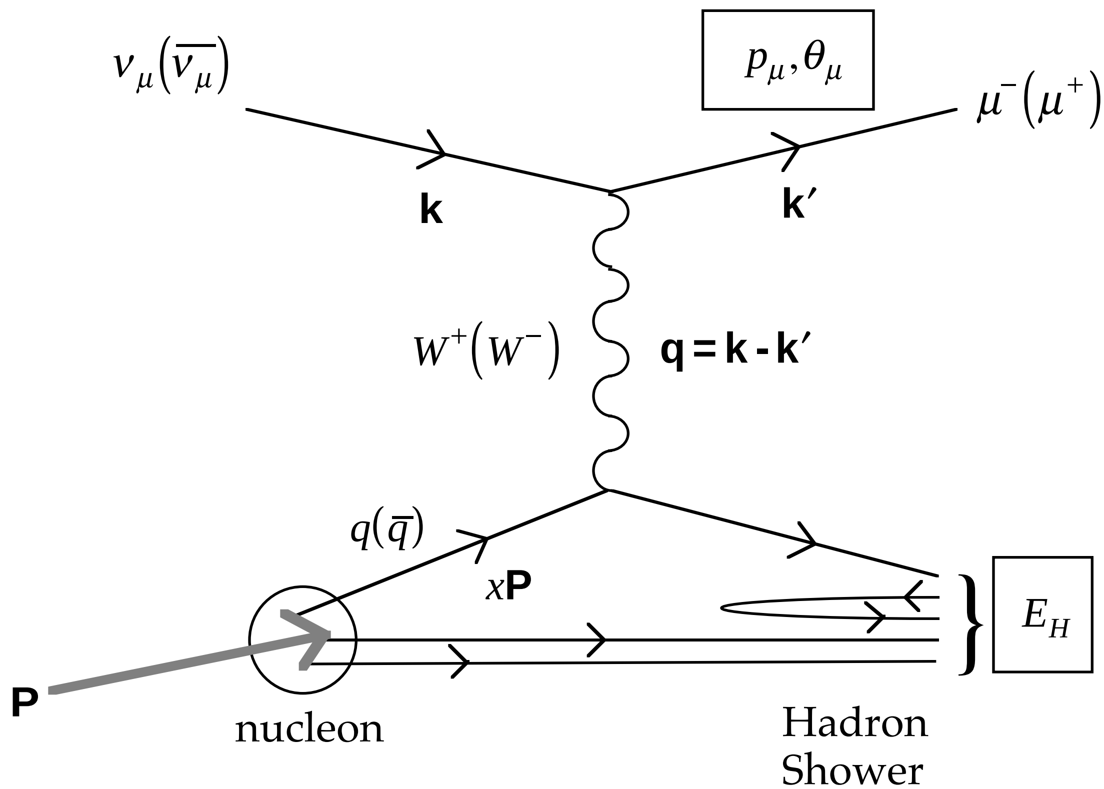

Figure 1.1: Kinematic variables of deep-inelastic scattering. A point-like constituent of the nucleon, a parton, carries a fraction *x* of the nucleon's momentum *p*. The measured experimental quantities are enclosed in rectangles.

$$k = \left(E_\nu, 0, 0, E_\nu\right) \tag{1.2}$$

$$k' = \left(E_\mu, p_\mu \sin\theta_\mu \cos\phi_\mu, p_\mu \sin\theta_\mu \sin\phi_\mu, p_\mu \cos\theta_\mu\right) \tag{1.3}$$

$$p = (M, 0, 0, 0) \tag{1.4}$$

$$p' = p + q = p + (k + k') \tag{1.5}$$

Lorentz-invariant variables commonly used to describe deep-inelastic scattering are derived as follows.

The square of the center of mass energy:

$$s = (p+k)^2 = M^2 + 2ME \tag{1.6}$$

The energy transferred to the hadronic system (the mass of the unobserved baryon is neglected):

$$\nu = \frac{p \cdot q}{M} = E_\nu - E_\mu = E_{HAD} \tag{1.7}$$

The negative square of the four-momentum transfer:

$$Q^2 = -q^2 = -(k-k')^2 = m_\mu^2 + 2E_\nu \left(E_\mu - p_\mu \cos\theta_\mu \right) \tag{1.8}$$

The invariant mass of the hadronic system:

$$W^2 = (p')^2 = (p+q)^2 = M^2 + 2M\nu - Q^2 \tag{1.9}$$

The Bjorken scaling variable, which represent the fractional momentum of the struck parton within the nucleon:

$$x = \frac{-q^2}{2p \cdot q} = \frac{Q^2}{2M\nu} \tag{1.10}$$

The inelasticity:

$$y = \frac{p \cdot q}{p \cdot k} = \frac{E_{HAD}}{E_\nu} \tag{1.11}$$

The inelasticity y is directly related to the lepton scattering angle θ^* in the center-of-mass frame:

$$y \approx 1 - \frac{1}{2}\left(1 + \cos\theta^*\right) \tag{1.12}$$

1.2.2 The Formalism of Deep-Inelastic Scattering

In this section the relationship between the structure functions and the neutrino-hadron cross-section is derived. The matrix element for the neutrino-hadron interaction can be written as [Rob90]:

$$\mathcal{M} = \frac{G_F}{\sqrt{2}} \frac{1}{1+Q^2/M_W^2} \underbrace{\bar{u}_\mu(k',s')\gamma_\alpha\left(1-\gamma_5\right)u_{\bar{\nu}}(k,s)}_{\text{lepton}} \underbrace{\left\langle X\middle|J_{CC}\middle|N;p,s\right\rangle}_{\text{hadron}} \tag{1.13}$$

where G_F is the weak coupling constant, M_W is the mass of the W-boson, (k,s) is the four-momentum and helicity of the incoming neutrino, (k',s') is the four-momentum and helicity of the outgoing muon, (p,s) is the four-momentum and helicity of the target nucleon, and $\bar{u}_\mu$ and $u_{\bar{\nu}}$ are the lepton spinors. The inclusive, spin-averaged cross-section proportional to $|\mathcal{M}|^2$ takes the form

$$\frac{d^2\sigma^{\nu N}}{d\Omega_\mu dE_\mu} = \frac{1}{\left(1+Q^2/M_W^2\right)^2} \frac{G_F^2}{2} \frac{m_\nu}{E_\nu} \frac{m_\mu}{E_\mu} \frac{E_\mu^2}{(2\pi)^2} L_{\alpha\beta} W^{\alpha\beta} \tag{1.14}$$

where E_ν and E_μ are the energies of the incident neutrino and final-state muon in the lab frame (nucleon at rest), and Ω is the solid angle into which the scattered muon lies. The leptonic tensor $L_{\alpha\beta}$ is given by

$$\begin{aligned} L_{\alpha\beta} &= \sum_{s,s'} \bar{u}_\mu(k',s')\gamma_\alpha(1-\gamma_5)u_\nu(k,s)\bar{u}_\nu(k,s)\gamma_\beta(1-\gamma_5)u_\mu(k',s') \\ &= \frac{2}{m_\nu m_\mu}\left[k'_\alpha k_\beta + k'_\beta k_\alpha - k\cdot k' g_{\alpha\beta} \mp i k^\gamma k'^\delta \varepsilon_{\gamma\delta\alpha\beta}\right] \end{aligned} \tag{1.15}$$

where the –(+) term applies to incident neutrinos (anti-neutrinos). The hadronic tensor $W^{\alpha\beta}$ is a second-rank tensor that parameterizes the unknown structure of the boson-nucleon vertex. There are only two independent vectors upon which $W^{\alpha\beta}$ can depend: p and q. Therefore the most general rank-2 tensor that can be constructed out of these two vectors is

$$
\begin{aligned}
W^{\alpha\beta} = & -g^{\alpha\beta} W_1 + \frac{p^\alpha p^\beta}{M^2} W_2 - \frac{i\varepsilon^{\alpha\beta\gamma\delta} p_\gamma q_\delta}{2M^2} W_3 \\
& + \frac{q^\alpha q^\beta}{M^2} W_4 + \frac{\left(p^\alpha q^\beta + p^\beta q^\alpha\right)}{M^2} W_5 \\
& + \frac{i\left(p^\alpha q^\beta - p^\beta q^\alpha\right)}{2M^2} W_6
\end{aligned}
\tag{1.16}
$$

where the *structure functions* W_i are real functions that depend only on q^2 and $p \cdot q$. In the limit of negligible quark masses,

$$
q^\alpha L_{\alpha\beta} = q^\beta L_{\alpha\beta} = 0 \tag{1.17}
$$

so that terms proportional to q^α or q^β in $W^{\alpha\beta}$ can be ignored; these are the coefficients of W_4, W_5, and W_6. After contracting the lepton and hadron tensors, Equation 1.14 becomes (neglecting Q^2 / M_W^2 and lepton masses):

$$
\frac{d^2\sigma^{\nu(\bar{\nu})N}}{d\Omega\, dE_\mu} = \frac{G_F^2}{2\pi^2} E_\mu^2 \left[\begin{aligned} & \cos^2\frac{\theta}{2} W_2^{\nu(\bar{\nu})N} + 2\sin^2\frac{\theta}{2} W_1^{\nu(\bar{\nu})N} \\ & \pm \frac{E_\nu + E_\mu}{M} \sin^2\frac{\theta}{2} W_3^{\nu(\bar{\nu})N} \end{aligned} \right] \tag{1.18}
$$

where the +(–) term corresponds to neutrino (anti-neutrino) scattering. In general, the structure functions $W_i\left(q^2, p \cdot q\right)$ depend on the target and may depend as well on the neutrino helicity. In terms of the absorption cross-sections for left-handed, right-handed, and scalar W bosons (σ_L, σ_R, σ_S) the structure functions can be written as:

$$W_1 = \frac{K}{\pi G_F \sqrt{2}}\left(\sigma_R + \sigma_L\right) \tag{1.19}$$

$$W_2 = \frac{K}{\pi G_F \sqrt{2}} \frac{Q^2}{Q^2 + \nu^2}\left(\sigma_R + \sigma_L + 2\sigma_S\right) \tag{1.20}$$

$$W_3 = \frac{K}{\pi G_F \sqrt{2}} \frac{2M}{\sqrt{Q^2 + \nu^2}}\left(\sigma_R - \sigma_L\right) \tag{1.21}$$

where K represents the flux of virtual *W*s. While there is some arbitrariness in the definition of K, the ratio of absorption cross-sections for longitudinally- to transversely-polarized bosons is well-defined:

$$R(\nu, Q^2) \equiv \frac{\sigma_S}{\sigma_T} = \frac{W_2}{W_1}\left(1 - \frac{\nu^2}{Q^2}\right) - 1 \tag{1.22}$$

In terms of the scaling variables x, y, and Q^2, Equation (1.18) becomes

$$\frac{d^2\sigma^{\nu(\bar{\nu})}}{dx\,dQ^2} = \frac{G_F^2}{2\pi x} E_\mu^2 \left[\left(1 - y - \frac{Mxy}{2E}\right) W_2^{\nu(\bar{\nu})} + y^2 x W_1^{\nu(\bar{\nu})} \pm y\left(1 - \frac{y^2}{2}\right) x \nu W_3^{\nu(\bar{\nu})}\right] \tag{1.23}$$

In the modern structure-function notation,

$$2xMW_1(\nu, Q^2) = 2xF_1(x, Q^2) \tag{1.24}$$

$$\nu W_2(\nu, Q^2) = F_2(x, Q^2) \tag{1.25}$$

$$x\nu W_3(\nu, Q^2) = xF_3(x, Q^2) \tag{1.26}$$

and so the differential cross-section takes the form

$$\frac{d^2\sigma^{\nu(\bar{\nu})}}{dx\,dy} = \frac{G_F^2 ME}{\pi}\left[\left(1-y-\frac{Mxy}{2E}\right)F_2^{\nu(\bar{\nu})} + \frac{y^2}{2}2xF_1^{\nu(\bar{\nu})} \pm y\left(1-\frac{y^2}{2}\right)\nu F_3^{\nu(\bar{\nu})}\right] \quad (1.27)$$

and

$$R(x,Q^2) = \frac{F_2}{2xF_1}\left(1-\frac{Q^2}{(2Mx)^2}\right)-1 \quad (1.28)$$

Equation 1.27 is the master equation of deep-inelastic neutrino and anti-neutrino scattering. It is the point where theory and experiment meet. That is, measurement of the deep inelastic differential cross-section is equivalent to a measurement of the structure functions. The structure functions contain all that can be known about the structure of the nucleon from deep-inelastic scattering.

R has been measured by other experiments and, in this analysis, the value of R used comes from a parameterization of the world's available data [Whi90b]. Hence Equation 1.27 can be expressed in terms of two unknown, measurable structure functions F_2 and xF_3:

$$\frac{d^2\sigma^{\nu(\bar{\nu})}}{dx\,dy} = \frac{G_F^2 ME}{\pi}\begin{bmatrix}\left(1-y-\frac{Mxy}{2E}+\frac{y^2}{2}\frac{1+4M^2x^2/Q^2}{1+R(x,Q^2)}\right)F_2^{\nu(\bar{\nu})} \\ \pm y\left(1-\frac{y^2}{2}\right)\nu F_3^{\nu(\bar{\nu})}\end{bmatrix} \quad (1.29)$$

This is the form of the differential cross-section used to extract the structure functions.

1.2.3 The Parton Model

The first experimental evidence that the proton is made of point-like constituents came from the large-Q^2 behavior of the structure functions. If two structureless particles scatter, the point "structure functions" are

$$2MW_1^{\text{point}}(\nu,Q^2)=\frac{Q^2}{2M\nu}\delta\left(1-\frac{Q^2}{2M\nu}\right) \tag{1.30}$$

$$\nu W_2^{\text{point}}(\nu,Q^2)=\delta\left(1-\frac{Q^2}{2M\nu}\right) \tag{1.31}$$

which have the property of being functions of a single dimensionless quantity, $Q^2/2M\nu$. Therefore, if large-Q^2 scattering begins to resolve point-like constituents inside the nucleon, the structure functions will begin to depend on a single dimensionless variable:

$$\lim_{\substack{Q^2\to\infty \\ x \text{ fixed}}} F_i(x,Q^2)=F_i(x) \tag{1.32}$$

This phenomenon is known as Bjorken scaling [Bjo69]. Early deep-inelastic scattering data verified that the structure functions become roughly independent of Q^2 above Q^2 = 1 GeV^2, in sharp contrast to the elastic form factors, which are strongly Q^2 dependent, falling like $1/Q^2$ below $Q^2 = 0.7\ GeV^2$.

Scaling of structure functions at high Q^2 is explained by the parton model. In this model, the nucleon is assumed to consist of point-like constituent partons. The deep-inelastic scattering environment is described by a highly relativistic frame, the "infinite momentum frame." In this highly-boosted frame, quarks interact among themselves on a time scale much longer than that of the collision, so the scattering is incoherent. Inelastic neutrino-nucleon scattering reduces to elastic scattering from free, individual partons. The partons are on-shell, the travel collinearly with the nucleon, and carry a fraction x of its momentum.

Elastic scattering of point particles depends only on the center-of-mass energy and the net angular momentum of the system. Neutrinos are left-handed and anti-neutrinos are right-handed. Considering spin-1/2 and spin-0 constituents in the nucleon, the possible helicity-dependent cross-sections for elastic neutrino-parton scattering are given by

$$\text{total spin } 0: \frac{d\sigma^{\nu q}}{d\cos\theta^*} = \frac{d\sigma^{\bar{\nu}\bar{q}}}{d\cos\theta^*} = \frac{G^2 M E_\nu}{\pi\left(1+Q^2 / M_W^2\right)^2} \tag{1.33}$$

$$\text{total spin } 1: \frac{d\sigma^{\nu\bar{q}}}{d\cos\theta^*} = \frac{d\sigma^{\bar{\nu}q}}{d\cos\theta^*} = \frac{G^2 M E_\nu}{\pi\left(1+Q^2 / M_W^2\right)^2}\left(\frac{1+\cos\theta^*}{2}\right)^2 \tag{1.34}$$

$$\text{total spin } \frac{1}{2}: \frac{d\sigma^{\nu k}}{d\cos\theta^*} = \frac{d\sigma^{\bar{\nu}k}}{d\cos\theta^*} = \frac{2G^2 M E_\nu}{\pi\left(1+Q^2 / M_W^2\right)^2}\left(\frac{\cos\theta^*}{2}\right)^2 \tag{1.35}$$

where θ^* is the muon's center-of-mass scattering angle. The superscripts identify the spin-1/2 partons with the quarks and anti-quarks. In principle, a spin-0 constituent may also be present, which is identified by the superscript k. As shall be seen, while the neutrino does not directly interact with a spin-0 component, the $p_\perp$ of the quark gives rise to an effective spin-0 component of the cross-section. The V–A structure of the weak interaction causes parity to maximally violated, so for massless partons only left-handed particles and right-handed anti-particles participate. Therefore, the four possible helicity configurations for high-energy neutrino-quark scattering are shown in Figure 1.2.

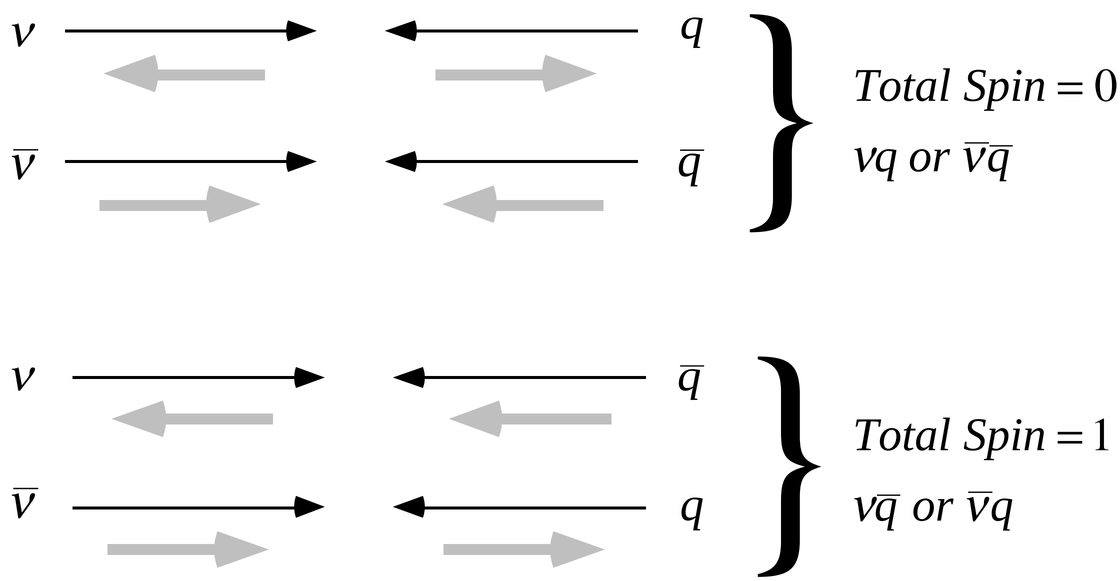

Figure 1.2: Possible helicity configurations for high-energy neutrinos and anti-neutrinos scattering from quarks and anti-quarks.

The probability of scattering from a particular type of parton is introduced with a parton distribution function $p(x)$. The quantity $p(x)dx$ is interpreted as the probability of finding a parton of type p in a hadron carrying a fraction x to $x + dx$ of the hadron's momentum. Then using the parton momentum distribution function $xp(x)$, the differential cross-section for scattering off one parton is

$$\frac{d^2\sigma}{dx\,dy} \propto \frac{G^2\, 2ME}{\pi\left(1 + Q^2 / M_W^2\right)^2} xp(x) \tag{1.36}$$

and gathering all contributions from the constituents of a target T, the cross-sections for neutrino and anti-neutrino scattering are

$$\frac{d^2\sigma^{\nu T}}{dx\,dy} = \frac{G^2 xs}{\pi\left(1 + Q^2 / M_W^2\right)^2}\left[q^{\nu T}(x) + (1-y)^2\,\bar{q}^{\nu T}(x) + 2(1-y)k^{\nu T}(x)\right] \tag{1.37}$$

$$\frac{d^2\sigma^{\bar{\nu}T}}{dx\,dy} = \frac{G^2 xs}{\pi\left(1+Q^2/M_W^2\right)^2}\left[\bar{q}^{\bar{\nu}T}(x) + (1-y)^2 q^{\bar{\nu}T}(x) + 2(1-y)k^{\bar{\nu}T}(x)\right] \qquad (1.38)$$

The parton distributions are associated with the structure functions by comparing the y dependencies of the above formulas with Equation 1.27, yielding

$$2xF_1^{\nu(\bar{\nu})T} = 2\left[xq^{\nu(\bar{\nu})T}(x) + x\bar{q}^{\nu(\bar{\nu})T}(x)\right] \qquad (1.39)$$

$$F_2^{\nu(\bar{\nu})T} = 2\left[xq^{\nu(\bar{\nu})T}(x) + x\bar{q}^{\nu(\bar{\nu})T}(x) + 2xk^{\nu(\bar{\nu})T}\right] \qquad (1.40)$$

$$xF_3^{\nu(\bar{\nu})T} = 2\left[xq^{\nu(\bar{\nu})T}(x) - x\bar{q}^{\nu(\bar{\nu})T}(x)\right] \qquad (1.41)$$

where the Q^2/M_W^2 and $Mxy/2E$ terms have been neglected. Thus, in the parton model, deep-inelastic structure functions are simply related to the momentum fractions of the partons in the target.

If the scattering were to take place exclusively from free spin-1/2 constituents, the Callan-Gross relation

$$2xF_1 = F_2 \qquad (1.42)$$

would be satisfied. However, at available energies, partons have non-negligible transverse momenta, which gives them apparent spin-0 behavior in the infinite-momentum-frame formalism. This leads to a difference between F_2 and $2xF_1$ that diminishes at higher Q^2.

The analogous expressions for electromagnetic charged-lepton scattering follow from the pure vector nature of the electromagnetic current. While neutrino scattering measures the helicity content of the nucleon, electromagnetic scattering measures the charge content:

$$2xF_1^{\ell T} = \sum_i e_i^2 \left[xq_i^{\ell T} + x\bar{q}_i^{\ell T} \right] \tag{1.43}$$

$$F_2^{\ell T} = \sum_i e_i^2 \left[xq_i^{\ell T} + x\bar{q}_i^{\ell T} + xk_i^{\ell T} \right] \tag{1.44}$$

where e_i is parton i's electric charge. There is no equivalent to the xF_3 term in electromagnetic interactions.

Neutrino scattering has the ability to resolve the flavor of the nucleon's constituents. The charge-current interaction changes the flavor of the struck quark, and conservation of charge at the quark vertex limits neutrinos to scatter from d, s, $\bar{u}$, and $\bar{c}$ quarks, and anti-neutrinos to scatter from $\bar{d}$, $\bar{s}$, u, and c quarks. Considering a parton target, the quark densities that contribute to the structure functions are

$$q^{\nu p}(x) = d^p(x) + s^p(x) \tag{1.45}$$

$$\bar{q}^{\nu p}(x) = \bar{u}^p(x) + \bar{c}^p(x) \tag{1.46}$$

$$q^{\bar{\nu} p}(x) = u^p(x) + c^p(x) \tag{1.47}$$

$$\bar{q}^{\bar{\nu} p}(x) = \bar{d}^p(x) + s^p(x) \tag{1.48}$$

Strong isospin invariance demands a symmetry between the proton and the neutron light quark densities:

$$d(x) \equiv d^p(x) = u^n(x) \tag{1.49}$$

$$\bar{d}(x) \equiv \bar{d}^p(x) = \bar{u}^n(x) \tag{1.50}$$

$$u(x) \equiv u^p(x) = d^n(x) \tag{1.51}$$

$$\bar{u}(x) \equiv \bar{u}^p(x) = \bar{d}^n(x) \tag{1.52}$$

Nucleons exhibit no net strangeness or charm, and these heavier flavors have isospin of zero. For this analysis, the following symmetries are assumed:

$$s(x) \equiv s^p(x) = s^n(x) \tag{1.53}$$

$$\bar{s}(x) \equiv \bar{s}^p(x) = \bar{s}^n(x) \tag{1.54}$$

$$c(x) \equiv c^p(x) = c^n(x) \tag{1.55}$$

$$\bar{c}(x) \equiv \bar{c}^p(x) = \bar{c}^n(x) \tag{1.56}$$

$$s(x) \equiv \bar{s}(x) \tag{1.57}$$

$$c(x) \equiv \bar{c}(x) \tag{1.58}$$

Using these symmetries, the quark distributions of the neutrino and the proton are described in terms of the proton quark distributions. All the parton distributions that follow are those for the proton.

$$q^{\nu n}(x) = u(x) + s(x) \tag{1.59}$$

$$\bar{q}^{\nu n}(x) = \bar{d}(x) + \bar{c}(x) \tag{1.60}$$

$$q^{\bar{\nu} n}(x) = d(x) + c(x) \tag{1.61}$$

$$\bar{q}^{\bar{\nu} n}(x) = \bar{u}(x) + \bar{s}(x) \tag{1.62}$$

Finally, the parton densities for an isoscalar nucleon, $N = 1/2 \times$ (proton + neutron), are

$$q^{\nu N}(x) = \frac{1}{2}\left[u(x) + d(x) + 2s(x)\right] \tag{1.63}$$

$$q^{\bar{\nu} N}(x) = \frac{1}{2}\left[u(x) + d(x) + 2c(x)\right] \tag{1.64}$$

$$\bar{q}^{\nu N}(x) = \frac{1}{2}\left[\bar{u}(x) + \bar{d}(x) + 2\bar{c}(x)\right] \tag{1.65}$$

$$\bar{q}^{\bar{\nu} N}(x) = \frac{1}{2}\left[\bar{u}(x) + \bar{d}(x) + 2\bar{s}(x)\right] \tag{1.66}$$

The quark content of the isoscalar structure function $2xF_1$ for neutrino scattering is obtained by substituting these densities into Equation 1.39:

$$\begin{aligned} 2xF_1^{\nu N}(x) &= 2xF_1^{\bar{\nu} N}(x) \\ &= xu(x) + x\bar{u}(x) + xd(x) + x\bar{d}(x) \\ &\quad + xs(x) + x\bar{s}(x) + xc(x) + x\bar{c}(x) \end{aligned} \tag{1.67}$$

The electromagnetic structure functions $2xF_1^{\ell p}$ and $2xF_1^{\ell n}$ are constructed from Equation 1.43 using the same parton densities as above and including the quark charges:

$$\begin{aligned} 2xF_1^{\ell p} &= \left(\frac{1}{3}\right)^2 \left[xd(x) + x\bar{d}(x) + xs(x) + x\bar{s}(x)\right] \\ &\quad + \left(\frac{2}{3}\right)^2 \left[xu(x) + x\bar{u}(x) + xc(x) + x\bar{c}(x)\right] \end{aligned} \tag{1.68}$$

$$\begin{aligned} 2xF_1^{\ell n} &= \left(\frac{1}{3}\right)^2 \left[xu(x) + x\bar{u}(x) + xs(x) + x\bar{s}(x)\right] \\ &\quad + \left(\frac{2}{3}\right)^2 \left[xd(x) + x\bar{d}(x) + xc(x) + x\bar{c}(x)\right] \end{aligned} \tag{1.69}$$

Thus $2xF_1^{\ell N}$ is given by

$$
\begin{aligned}
2xF_1^{\ell N} &= \left(2xF_1^{\ell p} + 2xF_1^{\ell n}\right)\Big/2 \\
&= \frac{5}{18}\left(xu + x\bar{u} + xd + x\bar{d}\right) \\
&+ \frac{1}{9}(xs + x\bar{s}) + \frac{4}{9}(xc + x\bar{c})
\end{aligned} \tag{1.70}
$$

Assuming that the value of $R = \sigma_L / \sigma_T$ is the same for the electromagnetic neutral-current and weak charged-current structure functions, the ratio of $2xF_1^{\ell N} \big/ 2xF_1^{\nu N}$ is equal to $F_2^{\ell N} \big/ F_2^{\nu N}$:

$$
\frac{F_2^{\ell N}}{F_2^{\nu N}} = \frac{5}{18}\left(1 - \frac{3}{5}\,\frac{xs + x\bar{s} - xc - x\bar{c}}{q + \bar{q}}\right) \tag{1.71}
$$

This relationship is known as the "5/18ths rule," and will be used in Chapter 8 to compare the charged-lepton structure functions to the results of this analysis.

The structure function xF_3, associated with the parity-violating weak interaction, represents the momentum density of valence quarks. Substituting the parton densities into Equation 1.41 yields

$$
xF_3^{\nu N} = xu_V(x) + xd_V(x) + 2xs(x) - 2xc(x) \tag{1.72}
$$

$$
xF_3^{\bar{\nu} N} = xu_V(x) + xd_V(x) - 2xs(x) + 2xc(x) \tag{1.73}
$$

where $u_V \equiv u - \bar{u}$ and $d_V \equiv d - \bar{d}$ are the proton's valence densities. The asymmetry of the *s*–*c* doublet results in $xF_3^{\nu N} \neq xF_3^{\bar{\nu} N}$. The method of extracting xF_3, described in Chapter 6, extracts the average of the neutrino and anti-neutrino distributions, so that

$$
xF_3(x) = \left(xF_3^{\nu N}(x) + xF_3^{\bar{\nu} N}(x)\right)\Big/2 = xu_V(x) + xd_V(x) \tag{1.74}
$$

1.2.4 The Theory of QCD

The parton model explains the scaling of the structure functions in terms of point-like constituents, but by itself offers no explanation for the dynamics between these constituents. If nucleons are made of quarks then how does one reconcile that quarks are never observed in isolation, yet when quarks participate in high-Q^2 scattering they behave like free particles? The need to refine the parton model was also apparent from detailed studies of structure functions, which found that scaling is only an approximation, and that logarithmic scaling violations are observed. QCD provides a consistent theory of quark dynamics, explains the scaling violations of the structure functions, and provides the detailed phenomenology of deep-inelastic scattering.

The behavior of quarks as quasi-free particles in high-Q^2 processes is accommodated by QCD's property of asymptotic freedom. Asymptotic freedom is a direct consequence of the non-Abelian structure of QCD. In a non-Abelian theory the gauge particles self-interact; that is, both the quarks and the gluon carry a color charge. Quarks are confined to hadrons because the self-interactions of the gluons tend to anti-screen a color charge, so that the strong force between two quarks increases as the distance between the two quarks gets larger. However, at shorter distances (equivalent to high Q^2), the strong coupling α_S decreases, so that as $Q^2 \to \infty$, $\alpha_S \to 0$.

1.2.4.1 Renormalization

When perturbatively calculating a cross-sections, the inclusion of higher-order diagrams leads to terms that are ultraviolet divergent. The purpose of renormalization is to remove these infinities in a systematic way. Renormalization [Alt82] involves introducing a free parameter μ^2, the renormalization scale, where μ has dimensions of mass. This scale is completely arbitrary, and different choices of μ^2 in the perturbative expansion are possible. The set of rules that specify the value of μ^2 for each divergent diagram describes the renormalization scheme that is used. The most commonly-used scheme is the modified minimum-subtraction ($\overline{\text{MS}}$) scheme, and in a minimal-subtraction scheme μ is chosen to be the same for every divergent integral.

A calculation of an observable quantity, like a cross-section, must be independent of these arbitrarily-chosen renormalization schemes and scales. This requirement is contained in the renormalization group equation

$$\mu \frac{d\mathcal{M}}{d\mu} = 0 \tag{1.75}$$

the renormalization group being the set of all rescalings of μ^2. To next-to-leading-order, the renormalization scale dependence of the strong coupling α_S is given by the beta function

$$\mu \frac{d\alpha_S\left(\mu^2\right)}{d\mu} = -\frac{\beta_0}{2\pi}\alpha_S^2\left(\mu^2\right) - \frac{\beta_1}{8\pi^2}\alpha_S^3\left(\mu^2\right) \tag{1.76}$$

where the coefficients are given by

$$\beta_0 = 11 - 2n_f/3 \tag{1.77}$$

$$\beta_1 = 102 - 38n_f/3 \tag{1.78}$$

and n_f is the number of quark flavors.

Solving Equation 1.76 for $\alpha_S(\mu^2)$ introduces one constant of integration, which may be denoted by $\alpha_S(\mu_0^2)$. This constant is the one fundamental constant of QCD, and it is determined by experiment: by measuring the strong coupling at one reference momentum scale μ_0^2. QCD then predicts how the coupling runs to any other scale according to Equation 1.76.

It is conventional to introduce the dimensional parameter Λ, and give the solution to Equation 1.76 in terms of it:

$$\alpha_S(\mu^2) = \frac{4\pi}{\beta_0 \ln\left(\mu^2/\Lambda^2\right)} \times \left[1 - \frac{\beta_1}{\beta_0^2} \frac{\ln\left[\ln\left(\mu^2/\Lambda^2\right)\right]}{\ln\left(\mu^2/\Lambda^2\right)}\right] \qquad (1.79)$$

Therefore, the measurement of Λ is equivalent to measuring $\alpha_S(\mu_0^2)$. Λ effectively sets the scale of the running coupling constant, and so it marks the boundary between quasi-free quarks and gluons and the hadronic bound states. Only for Q^2 values much larger than Λ, where the effective coupling is small, do perturbative techniques with quasi-free partons apply. If renormalization is carried out according to the $\overline{\mathrm{MS}}$ scheme, then Λ is referred to as $\Lambda_{\overline{\mathrm{MS}}}$.

1.2.4.2 Factorization

The connection between the quarks and the gluons and the physically-observed hadrons is established by the factorization theorem of QCD [Sop89]. The factorization theorem states that the structure functions can be decomposed into two parts, a parton distribution and a hard-scattering coefficient. The statement of the theorem is given by

$$W^{\alpha\beta}(q,p) = \sum_i \int_x^1 \frac{dz}{z} q_i^N(z,M) \hat{\omega}_i^{\alpha\beta}\left(q, zp, M, \alpha_S(\mu)\right) \qquad (1.80)$$

The sum is over all partons i. The parton-level hard-scattering coefficient $\hat{\omega}_i^{\alpha\beta}$ is a calculable function describing the probability for scattering to take place. The parton distribution function $q_i^N(z,M)$ is defined as before, where the index i indicates an individual type of parton, N refers to a given hadronic target, z is the fraction of the nucleon's momentum carried by parton i, and M is the factorization scale. The factorization scale M is distinguished from the renormalization scale μ because in principle they can be different.

The factorization theorem relies on QCD's property of asymptotic freedom, which permits high-energy scattering to be calculated using perturbation theory. The parton distribution function includes all the incalculable phenomena that occur at low energy scales—the infra-red dominated contributions. These are the interactions that bind the quarks and gluons into hadrons and are not amenable to perturbative calculations. The hard-scattering coefficient is sensitive only to momenta of order Q^2 and is ultraviolet dominated. The hard-scattering coefficients are calculable using QCD's Feynman rules. The scale M^2, therefore, sets the separation between the long-distance and short-distance parts of the process. A propagator that is off-shell by M^2 or more will contribute to the hard-scattering coefficient, and below the scale will contribute to the parton distribution. The factorization M^2 appears in the definition of the parton distributions in a similar way to the appearance of the renormalization scale μ^2 in the renormalization scheme.

Using the factorization theorem, the parton distributions can be determined experimentally. The structure functions in the hadronic tensor $W^{\alpha\beta}$ on the left-hand side of Equation 1.80 are measured and the hard-scattering coefficients on the right-hand side are calculated to a chosen order in perturbation theory, after making a choice of renormalization scheme. This way, the remaining unknown parton distributions are isolated. The parton distributions thus depend on the order and scheme used to determine them.

1.2.4.3 Evolution Equations

The parton distributions are infra-red dominated and perturbative QCD is unable to predict them outright. However, once the parton distributions are measured at one momentum scale, QCD predicts how they revolve to any other scale. The evolution of parton distributions is governed by the Dokshitzer-Gribov-Lipatov-Altarelli-Parisi evolution equations [Alt77, Dok78, Dok80, Gri72]:

$$\frac{dq^{NS}(x,M^2)}{d\ln M^2}=\frac{\alpha_S(\mu^2)}{2\pi}\int_x^1\frac{dy}{y}q^{NS}(y,M^2)\,P_{qq}\left(\frac{x}{y}\right) \tag{1.81}$$

$$\frac{dq^{S}(x,M^2)}{d\ln M^2}=\frac{\alpha_S(\mu^2)}{2\pi}\int_x^1\frac{dy}{y}\left[q^{S}(y,M^2)\,P_{qq}^{S}\left(\frac{x}{y}\right)+G(y,M^2)\,P_{qG}\left(\frac{x}{y}\right)\right] \tag{1.82}$$

$$\frac{dG(x,M^2)}{d\ln M^2}=\frac{\alpha_S(\mu^2)}{2\pi}\int_x^1\frac{dy}{y}\left[q^{S}(y,M^2)\,P_{Gq}\left(\frac{x}{y}\right)+G(y,M^2)\,P_{GG}\left(\frac{x}{y}\right)\right] \tag{1.83}$$

where

$$q^{NS}=\sum_i q^i-\bar{q}^i=u_V+d_V \tag{1.84}$$

$$q^{S}=\sum_i q^i+\bar{q}^i \tag{1.85}$$

G is the gluon distribution, and the "splitting functions" $P_{ij}(x/y)$ are the probability that parton *j* with momentum *y* will be resolved as parton *i* with momentum $x < y$. Thus the parton distributions evolve according to the radiative processes available to them. Note that the evolution of the non-singlet quark distribution q^{NS} does not depend on the gluon distribution. The diagrams for the leading-order splitting functions are shown in Figure

1.3, and the diagrams for the next-to-leading-order splitting functions are shown in Figure 1.4.

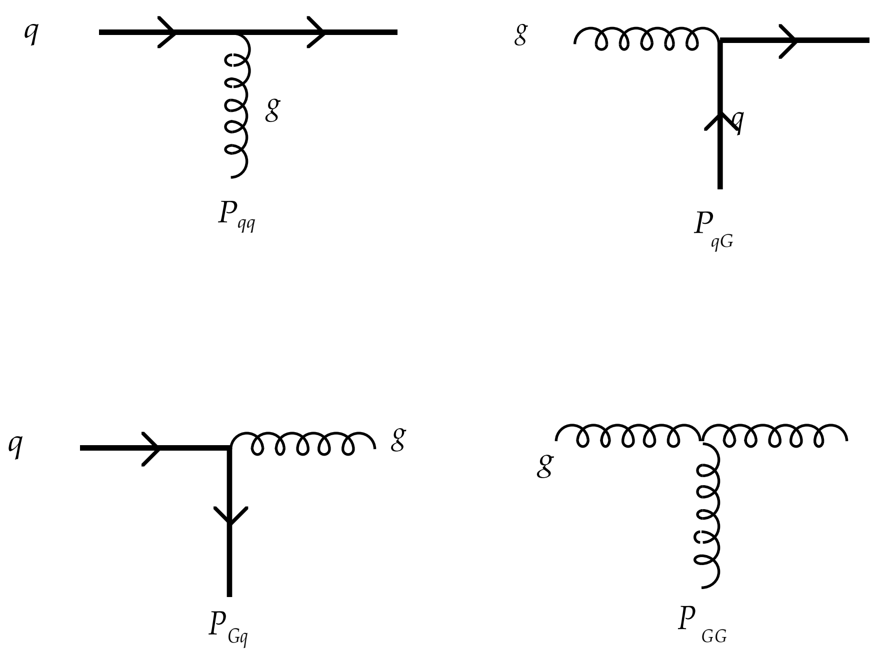

Figure 1.3: The leading-order splitting function diagrams.

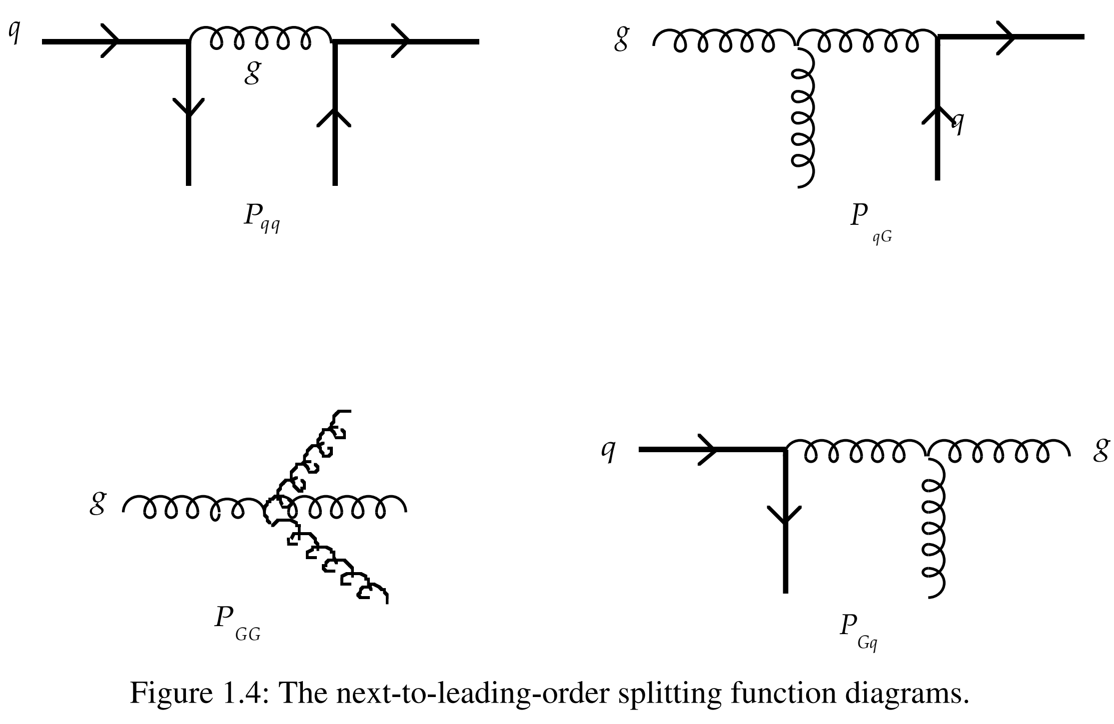

Figure 1.4: The next-to-leading-order splitting function diagrams.

1.2.4.4 Hard-Scattering Integrals

Using the factorization theorem of Equation 1.80, the measured structure functions are related to parton distributions, which evolve according to the evolution equations. The structure functions are found by convoluting the parton distributions with the hard-scattering coefficients:

$$F_3(x,Q^2) = \int_x^1 dy \left[C_3^q\left(\frac{x}{y}, M^2\right) q^{NS}(x, M^2) \right] \tag{1.86}$$

$$x^{-1}F_2(x,Q^2) = \int_x^1 dy \left[C_2^q\left(\frac{x}{y}, M^2\right) q^{S}(x, M^2) + C_2^G\left(\frac{x}{y}, M^2\right) G(x, M^2) \right] \tag{1.87}$$

where the C_i are the hard-scattering coefficients. The QCD behavior of the parton distributions—their evolution with scale—leads to the logarithmic scaling violations observed in the measurements of the structure functions.

The general relations between the partons and the structure functions given above simplify considerably at leading order. At leading order, the hard-scattering coefficients of the quark terms are proportional to $\delta(1 - x/y)$ and the coefficient of the gluon term vanishes. Hence, the leading-order quark assignments are simply $F_2 = q^S$ and $xF_3 = q^{NS}$. At NLO the parton assignments for the structure functions become more complicated and gluons are also involved.

1.2.4.5 QCD Scales

As with all applications of perturbative QCD, a theoretical uncertainty is associated with the choice of factorization and renormalization scales. A cross-section calculation done to all orders in α_S would be independent of scale. However, some scale dependence is unavoidable for any calculation done to finite order in α_S.

The choice of a scale when performing a calculation must be similar to a physical scale present in the process. In the case of deep-inelastic scattering, the μ^2 scale should be of order Q^2, the momentum transferred in the hard scattering. This is necessary because higher-order terms include logarithms proportional to $\ln(Q/\mu)$, and an unsuitably small choice of scale will mean that truncating these terms from the perturbative expansion is invalid. The convention is to choose $Q = \mu$ so that the $\ln(Q/\mu)$ terms vanish in all orders. It is also conventional to choose the factorization scale $M = \mu = Q$.

The error in the measurement of α_S due to the choice of the renormalization and factorization scales in deep-inelastic scattering has been investigated [Vir92, Mar91]. The results of those studies are included as a theoretical error in the measurement of α_S by this experiment (see Chapter 7).

1.3 Analysis Overview

1.3.1 The Data Sample

The CCFR collaboration performed two neutrino deep-inelastic scattering experiments at the Fermilab Tevatron. High-energy muon-type neutrinos and anti-neutrinos were provided using the Fermilab Quadrupole Triplet beamline, which focused pion and kaon secondaries produced in collisions of 800 *GeV* protons on a BeO target, before allowing them to decay in flight. Neutrino interactions were detected in the CCFR steel-scintillator target calorimeter, which was separated from the neutrino source by approximately one kilometer of earth and steel.

The unmagnetized CCFR target calorimeter is instrumented with liquid scintillator counters and drift chambers. In charged-current events, the angle of the muon and the total hadronic energy are measured in the target. The target is followed by a toroidal magnetic spectrometer, which includes drift chambers and provides the muon momentum measurement.

Approximately 3.7 million charged-current event triggers were analyzed. Since the flux of the neutrino beam cannot be directly measured, the flux is derived from a sample of events with low hadronic energy. From the flux and the number of observed events, the structure functions can be determined; about 950,000 neutrino-induced and 170,000 anti-neutrino-induced events were selected for inclusive nucleon structure-function measurements.

Once the structure functions are known, their Q^2 evolution can be compared against the theory of perturbative quantum chromodynamics. This yields a measurement of the QCD scale parameter Λ and hence the value of the strong coupling, α_S. The coupled evolution of the non-singlet and singlet quark distributions also yields a measurement of the gluon distribution.

1.3.2 Synopsis of This Thesis

The chapters of this thesis are organized as follows: The experimental setup, including the accelerator facilities at Fermilab and the CCFR detector, is described in Chapter 2. The calibration of the detector and the principles of event reconstruction are described in Chapter 3. Chapter 4 describes the corrections made to the data, including the corrections for detector acceptance and resolution. The flux extraction procedure is discussed in Chapter 5. The procedure for extracting structure functions, including the statistical and systematic errors, is described in Chapter 6. In Chapter 7 the structure functions are compared against the theory of QCD, and a precise measurement of $\alpha_S(M_Z^2)$ is made in the context of that theory. The structure functions and the QCD measurements are compared against measurements from other experiments in Chapter 8, which also presents the final conclusions of this thesis.

1.3.3 Prior Analyses

The structure-function analysis presented in this thesis is the latest in a series of analyses performed on neutrino data collected by the detector in Lab E at Fermilab. FNAL Experiment E616 [Mac84a, Pur84] used a narrow-band neutrino beam with a maximum incident proton energy of 400 *GeV*. The statistics of the experiment were limited by the low flux of the beam and the use of spark chambers, which could only record one neutrino event per "ping" in the accelerator cycle. E701 used the same beamline as E616, but added a second upstream detector to search for neutrino oscillations [Sto85]; a structure-function analysis on the combined E616/E701 data sample was also performed [Olt89].

In contrast, FNAL Experiments E744 and E770 were performed using the Tevatron, which provided an 800 *GeV* incident proton energy. The Quadrupole Triplet beamline provided a wide-band high-intensity beam of mixed neutrinos and anti-neutrinos. The statistics were further increased by replacing the spark chambers with drift chambers in the Lab E detector, which can record multiple events per ping.

A structure-function analysis on the combined E744/E770 data sample has previously been presented [Leu91, Qui92, Qui93]. The analysis in this thesis improves upon the previous analysis in several respects:

- The hadronic energy and muon energy calibrations now come directly from test beam data accumulated during the E744 and E770 neutrino runs. In the previous analysis, a technique called "relative calibration" was used to adjust the measured test beam calibrations. This technique was dropped for this analysis, since the results were shown to have large systematic uncertainties.

- The event analysis has been improved. In particular, the energy loss of the muon in the calorimeter is now more accurately modeled.

- The previous analysis used the radiative corrections due to de Rujula [Ruj79], which only included the effects of energy loss due to electromagnetic radiation by the outgoing muon. The present analysis uses the radiative corrections due to Bardin [Bar86], which includes the effects of electromagnetic interactions with the struck quark.

- In the previous analysis, the value of *R* used was that from a parameterization of data taken only at SLAC. The current analysis uses a value of *R* determined from a global fit the world's available measured data on *R* [Whi90b].

- The previous analysis used the strange sea determined from the E744 data only [Fou90]. The current analysis uses the strange sea determined from the combined E744 and E770 data sample [Rab93].

- The earlier analysis only presented the results of a non-singlet QCD evolution. This thesis also presents the results of a simultaneous QCD fit to the non-singlet and singlet structure functions, which not only reduces the statistical error on $\Lambda_{\overline{MS}}$, but also provides information on the gluon content of the proton.

- The previous analysis did not include higher-twist effects in the QCD fits, apart from correction for target mass. These effects are accounted for in the present analysis.

- The systematic error study has been expanded from the study presented in the previous analysis. In addition, the systematic errors have been incorporated into the QCD fits to produce a precise measurement of $\alpha_S(M_Z^2)$ from deep-inelastic scattering.